

A causal look into the quantum Talbot effect

A. S. Sanz* and S. Miret-Artés†

Instituto de Matemáticas y Física Fundamental, Consejo Superior de Investigaciones Científicas, Serrano 123, 28006 Madrid, Spain

(Dated: October 3, 2018)

A well-known phenomenon in both optics and quantum mechanics is the so-called Talbot effect. This near field interference effect arises when infinitely periodic diffracting structures or gratings are illuminated by highly coherent light or particle beams. Typical diffraction patterns known as quantum carpets are then observed. Here the authors provide an insightful picture of this nonlocal phenomenon as well as its classical limit in terms of Bohmian mechanics, also showing the causal reasons and conditions that explain its appearance. As an illustration, theoretical results obtained from diffraction of thermal He atoms by both N -slit arrays and weak corrugated surfaces are analyzed and discussed. Moreover, the authors also explain in terms of what they call the Talbot-Beeby effect how realistic interaction potentials induce shifts and distortions in the corresponding quantum carpets.

PACS numbers:

I. INTRODUCTION

Particle diffraction by different types of devices (slits, gratings, or surfaces) has become a standard technique to test the validity of quantum mechanics. This is confirmed by a large amount of experiments, ranging from tiny objects (e.g., electrons, neutrons, single atoms, or small clusters) to more complex, mesoscopic-size systems (e.g., fullerenes, large biomolecules, or Bose-Einstein condensates). Experiments with large, structured particles induce to think that, in principle, there are no size-dependent limits to observe particle diffraction, except those associated with the preservation of the system coherence. This is a very important issue, since the system coherence may disappear relatively fast as a consequence of the many eventual degrees of freedom involved in the process, either related to the surrounding environment (external) or associated with the own structure of the particle (internal).

In 1836, when characterizing optical gratings, Talbot¹ observed a repetition of alternate color bands of complementary colors (red-green and blue-yellow) at certain distances from the grating. About 50 years later, in 1881, Rayleigh² proved that this phenomenon is a consequence of the diffraction of highly spatially coherent (plane) waves by gratings; the color band structure observed is a manifestation of the periodicity and the shape of the grating. The alternation of complementary color bands occurs at integer multiples of $z_T = d^2/\lambda$, the *Talbot distance*, where d and λ are the grating period and the wavelength of the incident plane wave, respectively; bands with equal color patterns thus repeat at integer multiples of $2z_T$. The Talbot effect has important technological applications in optics, such as image processing and testing or production of optical elements. Similarly, its quantum-mechanical counterpart is relevant in electron optics, where it has many applications within electron microscopy. Moreover, this effect has been observed experimentally with heavy particles, such as Na atoms³

or Bose-Einstein condensates.⁴

Like in optics, N -slit arrays can also be considered typical examples of quantum gratings. When such arrays are illuminated by continuous, coherent wave fronts, a continuous quantum flow is observed behind the slits. This flow displays a typical pattern called *quantum carpet*⁵ with periodicity d along the direction parallel to the plane containing the slits (x) and $2z_T$ along the propagation direction (z). Full *recurrences* along z are found at integer multiples of z_T ; these recurrences are the direct analog of the color bands observed when working with optical gratings. A recurrence that coincides with the initial state describing the (diffracted) system is called a *revival* of such a state and appears at integer multiples of z_T ; for even integers, the state looks exactly the same as the initial one, while for odd integers it is shifted half a period ($d/2$) with respect to the latter. Recurrences at fractions of z_T consist of superposed images of the initial state with itself. Indeed, if the boundary conditions of the slits are “sharp” (the *window function* is not differentiable at the borders of the slit), one can observe *fractal* structures at irrational fractions of z_T , which give rise to *fractal carpets*.^{5,6,7,8,9}

The Talbot carpet associated with the diffraction of a monochromatic beam of He atoms ($E_z = 21$ meV, $\lambda = 2\pi\hbar/\sqrt{2mE_z} = 0.991$ Å) by a grating consisting of 50 Gaussian slits with period $d = 3.6$ Å is displayed in Fig. 1(a). Here, the x variable is normalized to the grating period, d , and the z variable to twice the Talbot distance $2z_T$, with $z_T = 13.08$ Å (throughout this work we will follow the same convention). The carpet appears when we record $\rho_t(x, z) = |\Psi_t(x, z)|^2$ along x at different times, monitored in terms of z (the wave propagates along the z direction at a constant speed $v_z = 2\pi\hbar/m\lambda$; see below for details). That is, at a given time t_{plot} we have plotted the “slice” $\rho_{t_{\text{plot}}}(x, z_{\text{plot}})$ of the probability density, where x runs over all possible values along a certain range (in the figure, from -6 to 6) and the z value is fixed: $z_{\text{plot}} = z(t_{\text{plot}}) = v_z t_{\text{plot}}$. Some of these

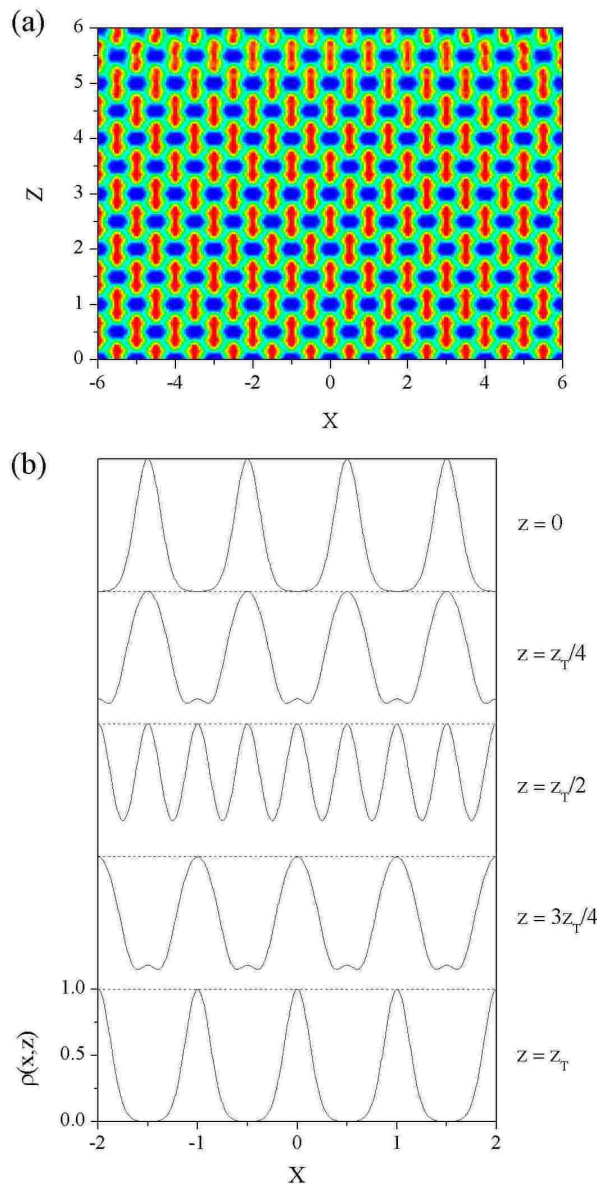


FIG. 1: (Color online) (a) Quantum carpet for He diffracted by a 50-slit array. The color scale, from blue to red, indicates increasing values of the probability density. (b) Snapshots of the probability density from $z = 0$ to $z = z_T$. In both panels, the x distance is scaled in units of the grating period d and z in units of twice the Talbot distance ($2z_T = 2d^2/\lambda$).

slices are shown individually in Fig. 1(b), from $z = 0$ to $z = z_T$. As mentioned above, revivals of the initial state occur at z_T (shifted half a period), while the other slices manifest vague reminiscences of $\rho_0(x, 0)$. After reaching $z = z_T$, the diffracted beam will evolve towards $2z_T$ following the inverse sequence to that shown in Fig. 1(b) [see Fig. 1(a)], then an exact revival of the initial probability distribution will be observed. This process repeats endlessly unless the grating has a finite size. With real gratings its extension is limited to distances of the order

of the grating size. At such distances the carpet gradually fades, and the typical Fraunhofer patterns that characterize most particle diffraction experiments start becoming apparent.

Although Talbot patterns are well known in the literature, as far as we know there is no detailed explanation for them in causal terms. This work is aimed to provide a full causal interpretation for this phenomenon as well as for its relationship with the Fraunhofer diffraction and the classical limit. For this purpose, we have chosen Bohmian mechanics, where the standard wave picture is replaced by trajectories in configuration space. The use of such trajectories is very important in order to shed some light into real experiments, where a picture in terms of the motion of individual particles is always highly desirable (specially if particles follow the quantum flow, unlike other classical representations). This is an important issue, for instance, in surface science experiments, where the illumination of a surface for its study and characterization is limited in extension. Note that, when assuming that no imperfections are present, surfaces can be considered as gratings analogous to N -slit arrays because of their periodicity. Nonetheless, the short-range attractive interaction undergone by the diffracted particles near the surface leads to a slight shift and distortion of the Talbot period. We have called this effect the *Talbot-Beeby effect* since the variation of the diffracted beam wavelength due to presence of attractive wells is known as the *Beeby correction*¹⁰ in surface scattering.

This work is organized as follows. In order to be self-contained, a rigorous mathematical approach in terms of standard quantum mechanics will be presented in Sec. II, analyzing both the appearance of the Talbot effect in gratings of Gaussian slits and the transition to the Fraunhofer regime. In Sec. III we describe the application of Bohmian mechanics to the problems discussed in the previous section. A discussion of the Talbot and Talbot-Beeby effects in diffraction of He atoms by both an N -slit array and the Cu(110) surface is given in Secs. IV and V, respectively. In the light of these results, the meaning of the classical limit and the quantum-classical correspondence is discussed in Sec. VI. Finally, the main conclusions from this work are summarized in Sec. VII.

II. WAVE APPROACH TO THE TALBOT EFFECT

Rigorous analytical studies of the Talbot effect from an optical viewpoint can be found, for instance, in Ref. 11. Here we provide an alternative quantum-mechanical derivation highlighting the physical aspects underlying this phenomenon, in particular, (i) the role of the superposition principle and (ii) the analogy/equivalence between Talbot patterns and the carpets observed in multi-mode cavities (e.g., waveguides). For simplicity, we focus on gratings constituted by Gaussian slits,^{12,13} i.e., characterized by Gaussian transmission functions, though our

analysis can be straightforwardly generalized to any kind of periodic grating. Gaussian transmissions can be observed, for instance, when studying the diffraction of a monochromatic beam (with wavelength λ) by a soft, repulsive (exponential) potential barrier with an infinity of identical holes (slits).¹³

1. Single Gaussian slit

To understand the physics associated with the time evolution of the diffracted wave function by an infinite Gaussian grating, it is important to consider first the dynamics of a single diffracted Gaussian function. Assuming the initial time ($t = 0$) as the instant when the incident wave has just passed through the slit with perpendicular velocity ($v_x = 0$), the initial state can be expressed as

$$\Phi_0(x, z) = A(0) e^{-x^2/4\sigma_x^2 - z^2/4\sigma_z^2 + ip_z z/\hbar}, \quad (1)$$

where $A(0) = (2\pi\sigma_x\sigma_z)^{-1/2}$ is the norm and σ_x and σ_z the initial widths in the x and z directions, respectively. Within this description, note that σ_x is related to the transmission function of the slit, giving an idea of the aperture dimension (i.e., the slit width); on the other hand, σ_z is an indicator of the monochromaticity of the incident beam (the limit $\sigma_z \rightarrow \infty$ represents the case of a fully monochromatic incident wave).

The time propagation of Φ_0 is given by

$$\Phi_t(x, z) = A(t) e^{-x^2/4\tilde{\sigma}_{x,t}\sigma_x - (z-z_t)^2/4\tilde{\sigma}_{z,t}\sigma_z} \times e^{ip_z(z-z_t)/\hbar + iE_z t/\hbar}, \quad (2)$$

with $A(t) = (2\pi\tilde{\sigma}_{x,t}\tilde{\sigma}_{z,t})^{-1/2}$, $z_t = v_z t$, $E_z = p_z^2/2m$, and

$$\tilde{\sigma}_{i,t} = \sigma_i \left(1 + \frac{i\hbar t}{2m\sigma_i^2} \right), \quad i = x, z, \quad (3)$$

where

$$\sigma_{i,t} = |\tilde{\sigma}_{i,t}| = \sigma_i \sqrt{1 + \frac{\hbar^2 t^2}{4m^2 \sigma_i^4}}, \quad i = x, z \quad (4)$$

gives the instantaneous width along each direction. From Eq. (4) a time scale $t_s = 2m\sigma_i^2/\hbar$ separating two regimes with different “spreading rates” can be defined. If $t \ll t_s$, the Gaussian widths almost remain the same ($\sigma_{i,t} \approx \sigma_i$). On the other hand, if $t \gg t_s$, the Gaussian widths undergo a linear increase with time ($\sigma_{i,t} \approx \hbar t/2m\sigma_i$). In this way, choosing $\sigma_x = d/8$ and $\sigma_z = d$, Φ_t will not almost display any increase in its size along z , but only along x . Accordingly, Eq. (2) can be reexpressed as

$$\Phi_t(x, z) = A'(t) e^{-x^2/4\tilde{\sigma}_{x,t}\sigma_x - (z-z_t)^2/4\sigma_z^2} \times e^{ip_z(z-z_t)/\hbar + iE_z t/\hbar}, \quad (5)$$

where $A'(t) = (2\pi\tilde{\sigma}_{x,t}\sigma_z)^{-1/2}$. Note that this will ensure the overlapping of Gaussian functions (along the x direction) in the case of the grating, and therefore the appearance of interference.

For hard slits, the interaction potential is zero everywhere except along the grating ($z = 0$), where it is infinity. Thus, there is no coupling between both coordinates, x and z , and the time evolution of the wave function along each direction can be studied separately. Since the interference takes place along x , we will only focus on the part of the wave function depending on this variable,

$$\phi_t(x) = A_x(t) e^{-x^2/4\tilde{\sigma}_{x,t}\sigma_x}, \quad (6)$$

where $A_x(t) = (2\pi\tilde{\sigma}_{x,t}^2)^{-1/4}$. Regarding the component of the wave function along z , it is only important to know that it propagates at a constant speed v_z , i.e., its centroid evolves according to $z(t) = v_z t$. This allows to simplify our analysis, reducing it to a one-dimensional time-dependent problem, where the z coordinate contains the same information as t . Thus, from now on the subscript x will be dropped from the magnitudes related to the spreading along the x direction (σ and A instead of σ_x and A_x , respectively), and from the momentum associated with the x coordinate (p instead of p_x).

2. Infinite periodic slit gratings

According to Bloch’s theorem,¹⁴ the problem of finding the diffracted wave function associated with a given infinite periodic potential reduces to determining the wave function associated with a single *unit cell* of such a potential; the full wave function is just a repetition of the latter, which satisfies the following Born-von Karman boundary conditions:

$$\psi_t(x+d) = \psi_t(x). \quad (7)$$

Thus, we assume that the total number of Gaussian slits amounts to $N = 2K + 1$, the slits being centered at $x_0^{(k)} = kd$ (with $k = 0, \pm 1, \pm 2, \dots, \pm K$) and $z_0^{(k)} = 0$. Our problem then reduces to only consider one of the Gaussian wave packets ϕ_t , constituting the full wave function. We can choose, for instance, ϕ_t to be the wave packet with $k = 0$, which is confined within the space region $x = \pm d/2$ and whose time evolution is described by Eq. (6). In direct analogy to surface science, from now on we will call the space region of length d enclosing each (initial) Gaussian wave packet [i.e., $(k-1)d/2 \leq x \leq kd/2$] a unit cell.

As is well known, any unbound wave function can be represented as a superposition of plane waves,

$$\phi_t(x) = \frac{1}{\sqrt{2\pi\hbar}} \int a(p) e^{ipx/\hbar - i\omega t} dp, \quad (8)$$

with

$$a(p) = \frac{1}{\sqrt{2\pi\hbar}} \int \phi_0(x) e^{-ipx/\hbar} dx. \quad (9)$$

Thus, Eq. (6) can be expressed as

$$\phi_t(x) = \frac{(8\pi\sigma^2)^{1/4}}{2\pi\hbar} \int e^{-\sigma^2 p^2/\hbar^2 + ipx/\hbar - i\omega t} dp. \quad (10)$$

Because of the periodic boundary condition (7), not all momenta are allowed; we then pass from a continuous basis of momenta to a discrete one, and Eq. (10) becomes

$$\phi_t(x) = \sqrt{\frac{1}{d}} \left(\frac{8\pi\sigma^2}{d^2} \right)^{1/4} \sum_{|n|=1}^{\infty} e^{-\sigma^2 p_n^2/\hbar^2 + ip_n x/\hbar - i\omega_n t}, \quad (11)$$

where $p_n = 2\pi\hbar n/d$ and $\omega_n = 2\pi^2\hbar n^2/md^2$.

The initial (full) wave function describing the system (along the x direction) is assumed to be a coherent, nonoverlapping superposition of identical Gaussian wave functions that propagate along the z direction with constant velocity,

$$\psi_0(x) \propto \lim_{K \rightarrow \infty} A(0) \sum_{k=-K}^K e^{-(x-kd)^2/4\sigma^2}. \quad (12)$$

The corresponding time-evolved wave function is straightforwardly obtained by replacing the Gaussian wave packets in Eq. (12) by their time-dependent counterparts given by Eq. (11). This leads to

$$\psi_t(x) \propto \lim_{K \rightarrow \infty} (2K+1) \phi_t(x) \quad (13)$$

after rearranging terms. As one would expect, Eq. (13) indicates that all the information regarding the infinite grating is contained within a single unit cell, with the factor $2K+1$ arising from the total number of unit cells considered. To avoid the divergence introduced by this factor, we reexpress Eq. (13) as

$$\psi_t(x) = \lim_{K \rightarrow \infty} \frac{A(t)}{2K+1} \sum_{k=-K}^K e^{-(x-kd)^2/4\tilde{\sigma}_t^2}. \quad (14)$$

The smallest time elapsed necessary to observe a recurrence of the wave function is determined by the condition

$$\psi_{t+\tau_r}(x) = \psi_t(x). \quad (15)$$

Using Eq. (11), it is straightforward to see that this condition is satisfied whenever $e^{-i\omega_n \tau_r} = e^{-2\pi i}$ for all n , i.e., when $\tau_r = 2\pi/\omega_1 = md^2/\pi\hbar$. At this time, the z distance between two consecutive recurrences of ϕ_t will be $z_r = v_z \tau_r = 2d^2/\lambda$, i.e., twice the Talbot distance ($2z_T$). As shown in Fig. 1(b), there are also recurrences with periodicity $z_r = d^2/\lambda = z_T$. These recurrences result from considering the symmetry

$$\psi_{t+\tau_r/2}(x + d/2) = \psi_t(x), \quad (16)$$

which appears when taking the terms $e^{ip_n x/\hbar - i\omega_n \tau_r}$ as a whole.

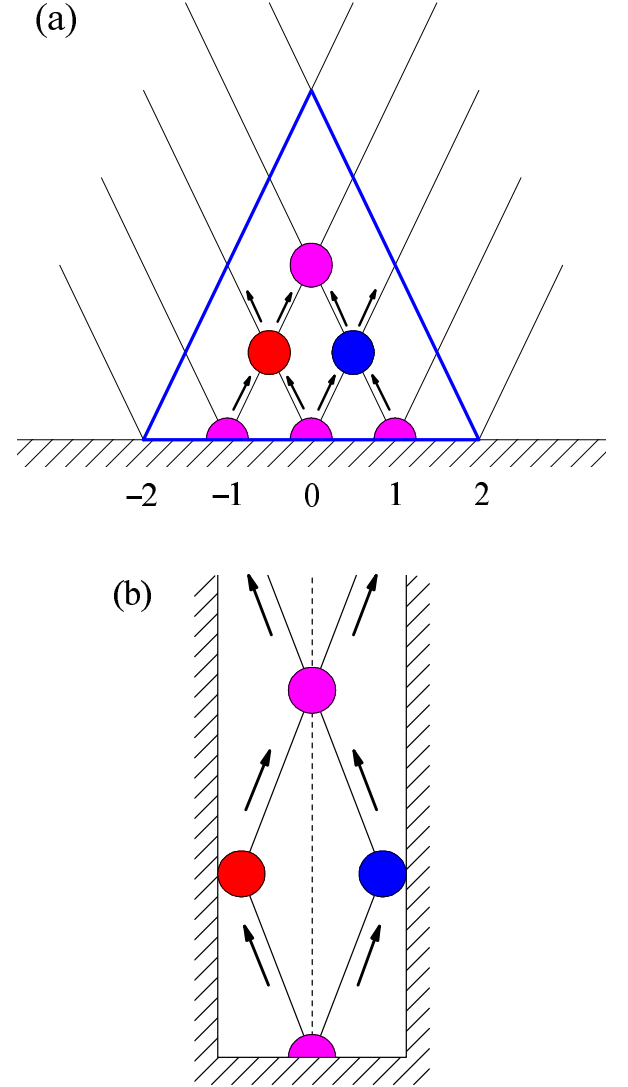


FIG. 2: (Color online) Schematic picture of the formation of revivals in (a) gratings of Gaussian slits and (b) multimode cavities. Arrows indicate the direction of the motion of the “interfering” disks (see text for details) and straight lines represent the corresponding paths. In part (a), the numbers label different slits, and the blue line limits the Talbot region.

The observation of revivals can be explained by means of a simple schematic picture, which is displayed in Fig. 2(a). To understand this picture we consider that each wave packet can be represented by two “interfering” hard disks that propagate along the z direction with opposite x velocities (the x motion of the center of mass is null, as expected from the propagation of a real wave packet, which only advances along z). These disks thus indicate the spreading of the wave packet. Following the motion of the disks associated with $k=0$, we observe that they meet at $x = \pm d/2$ and $z = z_T$ with those arriving from the neighboring slits ($k = \pm 1$). Since all disks are identical, there will be full constructive “interference”, this leading to the first revival. The next revival

will occur at $z = 2z_T$ and is caused by the interference of the disks coming from $k = \pm 1$, but not from $k = 0$; the disks leaving the slit with $k = 0$ will contribute to the revivals observed at $x = \pm d$ and $z = 2z_T$.

From Fig. 2(a) we can also infer an effective size for Talbot structures when the grating periodicity is limited. In the picture we have represented five slits; thus, after the ingoing-moving disks corresponding to $k = \pm 2$ have interfered, no Talbot revivals will be observed. From the point of view of Gaussian wave packets, this will happen after the size of those corresponding to the outermost slits is large enough as to make them to interfere, i.e., when $2\sigma_t \approx 2Kd$. Assuming that at that stage the width of the Gaussian functions increases linearly with time, i.e., $\sigma_t \approx \hbar t / 2m\sigma$, the maximum time at which a (partial) revival can be observed is $t_{\max} \approx 2Kdm\sigma/\hbar$. Since the propagation along z is also linear with time (at the speed v_z), the z distance where such a revival will be observable is

$$z_{\max} \approx v_z t_{\max} \approx 2z_T \frac{\pi(N-1)}{8} \quad (17)$$

(we have particularized this expression to our case, where $\sigma = d/8$). Examples of the validity of this relation will be seen in Sec. IV. Beyond z_{\max} a transition towards the Fraunhofer diffraction regime, with its characteristic fringe patterns, starts to be observed. This transition takes place beyond the boundaries of the Talbot region, enclosed in Fig. 2(a) by a blue triangle with height z_{\max} and basis $(N-1)d$.

As soon as the wave function (or part of it) leaves the Talbot region, Bloch's theorem (and therefore the Born-von Karman boundary conditions) is no longer applicable. To describe the Fraunhofer diffraction, one has to start from Eq. (14), but having in mind that the grating has a finite size. Thus, at a relatively long z distance from the grating, its dimensions are negligible when compared with the x distances involved in the diffraction process [i.e., $x \gg (N-1)d$], and therefore

$$e^{-(x-kd)^2/4\tilde{\sigma}_t\sigma} \approx e^{-\sigma^2\kappa^2x^2/z^2} e^{i\kappa x^2/2z} e^{-i\kappa kdx/z}, \quad (18)$$

where $\kappa = 2\pi/\lambda$. Substituting the right hand side of this expression into Eq. (14) we obtain

$$\psi_t(x) \approx \frac{A(t)}{2K+1} e^{-\sigma^2\kappa^2x^2/z^2} e^{i\kappa x^2/2z} \sum_{k=-K}^K e^{-i\kappa kdx/z}. \quad (19)$$

Now, using the so-called paraxial approximation from optics¹⁵ and considering $x/z = \tan\theta \approx \sin\theta$ (θ is the observation angle), the probability density (diffraction pattern) along x can be expressed as

$$\varrho_t(x) = |A(t)|^2 e^{-\sigma^2\kappa^2x^2/z^2} \left[\frac{\sin(N\kappa d \sin\theta/2)}{N \sin(\kappa d \sin\theta/2)} \right]^2. \quad (20)$$

In this expression, the term between square brackets is the *structure factor*, which accounts for the interference

among the different diffracted (Gaussian) beams. On the other hand, the normalized exponential is the *form factor*, which is related to the diffraction by a single unit cell. Because of the information provided by these factors, they are very useful to characterize optical grids¹⁵ as well as periodic surfaces.¹⁴

From the structure factor we note that the Fraunhofer fringes appear in accordance to the diffraction (quantization) condition

$$\sin\theta = \ell \frac{\lambda}{d}, \quad \ell = 0, \pm 1, \pm 2, \dots \quad (21)$$

where ℓ is the *diffraction order*. On the other hand, there will be a series of minima whenever

$$\sin\theta = \frac{\ell'}{N} \frac{\lambda}{d}, \quad |\ell' - \ell| = 1, 2, \dots, N-1. \quad (22)$$

As seen, there are $N-1$ minima between two consecutive principal maxima and, consequently, $N-2$ secondary maxima; the height of the latter is smaller than that of the principal maxima and decreases¹² very fast with N .

Finally, a comment regarding the local spreading of each Gaussian wave packet and the boundary condition Eq. (7) is worth stressing. According to Eq. (6), after a certain time the size of every Gaussian in (14) at $t = 0$ will be such that it will extend beyond the boundaries of its corresponding unit cell. That is, the spreading of ϕ_t , which is a local property, gives rise to the appearance of a nonlocal behavior, where each part of the resulting wave function, ψ_t , is strongly influenced by the presence of the remaining ones. Note, indeed, that the Talbot effect is precisely a nonlocal effect: it emerges as a consequence of the overlapping of many identical wave packets. As will be seen below, Bohmian mechanics provides a natural picture to this problem in terms of the regimes of motion associated with two well-defined dynamic equilibria.

3. Multimode cavities

The Talbot effect is closely related to multimode interference,^{16,17,18} the interference process that takes place when an infinity of modes of a cavity are superposed. Waveguides are a typical example of multimode cavity where the wave motion is constrained along one direction (e.g., x) and unbound along the other (e.g., z). Assuming no coupling between the motion along each direction, and that the cavity is a square box along x , centered at $x = 0$ and with length d , the time evolution of a Gaussian wave packet can be expressed at any time in terms of the modes corresponding to this cavity as

$$\begin{aligned} \phi_t(x) &= \sqrt{\frac{8}{d}} \left(\frac{2\pi\sigma^2}{d^2} \right)^{1/4} \\ &\times \sum_{n=0}^{\infty} e^{-\sigma^2 p_n^2/\hbar^2 - iE_n t/\hbar} \cos(p_n x/\hbar), \quad n = 0, 1, 2, \dots \end{aligned} \quad (23)$$

with $p_n = (2n + 1)\pi\hbar/d$ and $E_n = p_n^2/2m$. It is easy to show¹⁹ that recurrences in the probability density arising from Eq. (23) occur at integer multiples of the period associated with the smallest frequency. In our case, this frequency is $\omega_{1,0} = (E_1 - E_0)/\hbar = 4\pi^2\hbar/md^2$, and the period associated is

$$\tau_r = \frac{2\pi}{\omega_{1,0}} = \frac{md^2}{2\pi\hbar}. \quad (24)$$

We have to mention that the same periodicity can also be observed in the wave function, except for a constant phase factor $[\phi_{t+\tau_r}(x) = e^{i\varphi}\phi_t(x)]$.

Since the wave function evolves at a constant speed along z , the recurrences will also give rise to the formation of quantum carpets; some examples of these carpets can be found, for instance, in Ref. 12. These recurrences appear at integer multiples of the distance $z_r = v_z\tau_r = d^2/\lambda$, which corresponds to the Talbot distance obtained in the case of a periodic grating. This is the analogous case to the revivals observed at $z = 2z_T$ in grating systems. To understand why the same type of recurrences cannot be observed in both periodic gratings and cavities, it is very instructive to look at the scheme represented in Fig. 2(b). This picture is equivalent to that shown in Fig. 2(a), but with the difference that the only possibility for the disks to cross is when they meet again; no interference at $x = \pm d/2$ is possible. In other words, while the quantization leading to Eq. (11) arises from a “matching” condition at the borders of neighboring unit cells (thus allowing interference), in Eq. (23) it comes from having impenetrable boundaries.

III. BOHMIAN APPROACH TO THE TALBOT EFFECT

The fundamental equations of Bohmian mechanics are commonly derived by expressing the system wave function in polar form,^{20,21,22}

$$\Psi_t(x, z) = \rho_t^{1/2}(x, z) e^{iS_t(x, z)/\hbar}. \quad (25)$$

Here, ρ_t is the probability density and S_t is the (real-valued) phase. Substituting Eq. (25) into the time-dependent Schrödinger equation and making a bit of algebra, one reaches two (real-valued) coupled differential equations

$$\frac{\partial \rho_t}{\partial t} + \nabla \cdot \left(\rho_t \frac{\nabla S_t}{m} \right) = 0, \quad (26)$$

$$\frac{\partial S_t}{\partial t} + \frac{(\nabla S_t)^2}{2m} + V + Q_t = 0. \quad (27)$$

Equation (26) is a continuity equation that ensures the conservation of the quantum particle flux. On the other hand, Eq. (27), more interesting from a dynamical viewpoint, is a quantum Hamilton-Jacobi equation governing the particle motion under the action of a total effective

potential $V_t^{\text{eff}} = V + Q_t$. The last term in the left hand side of this equation is the so-called *quantum potential*

$$Q_t = -\frac{\hbar^2}{2m} \frac{\nabla^2 \rho_t^{1/2}}{\rho_t^{1/2}}. \quad (28)$$

This context-dependent, nonlocal potential determines together with V the total force acting over the system.

In the classical Hamilton-Jacobi theory ($Q_t = 0$), S_t represents the action of the system at a time t , and the trajectories describing the evolution of the system correspond to the paths perpendicular to the constant-action surfaces at each time. Similarly, since the Schrödinger equation can be rewritten in terms of the Hamilton-Jacobi equation (27), S_t can be interpreted as a quantum action satisfying similar mathematical requirements as its classical homologous. In Bohmian mechanics the classical-like concept of trajectory thus emerges in a natural manner; particle trajectories are defined as the solutions of the equation of motion

$$\dot{\mathbf{r}} = \frac{\nabla S_t}{m} = \frac{\hbar}{m} \text{Im} [\Psi_t^{-1} \nabla \Psi_t]. \quad (29)$$

Moreover, since in Bohmian mechanics the system consists of a wave and a particle, it is not necessary to specify the initial momentum for each particle (as happens in classical mechanics), but only its initial position, $\mathbf{r}_0 = (x_0, z_0)$, as well as the initial wave function Ψ_0 . The initial momentum field is predetermined by Ψ_0 via Eq. (29), and the statistical predictions of the standard quantum mechanics are reproduced by considering an ensemble of (noninteracting²³) particles distributed according to the initial probability density $\rho_0 = |\Psi_0|^2$.

Equation (29) is well defined provided the wave function is continuous and differentiable. This is not the case, however, for quantum fractals,^{6,7,8,9} where the Bohmian mechanics based on Eq. (29) is unable to offer a trajectory picture for the corresponding wave functions. This apparent incompleteness can be nevertheless “bridged” by taking into account the decomposition of the quantum fractal as a sum of (differentiable) eigenvectors of the Hamiltonian, and then redefining Eq. (29) conveniently. This is seen in detail in Ref. 19, where a generalization of the standard formulation of Bohmian mechanics to include quantum fractals is given.

Prior to any calculation, some physical insight into slit diffraction problems is possible by studying the properties of the velocity field. Indeed, the fact that Bloch’s theorem (together with the Born-von Karman boundary conditions) holds simplifies this study from both a conceptual and a computational perspective. Conceptually, because the study of the full system reduces to only understanding the dynamics within a single unit cell. In this sense, the analysis is similar to that of having a multimode cavity, as said above. This implies a computational advantage: it allows to perform calculations taking into account only what happens inside a single unit cell and periodic boundary conditions [i.e.,

$\psi_t(x-d/2) = \psi_t(x+d/2)]$, thus reducing the computation efforts. Of course, this simplification is only possible if we are under the assumption of infinite periodic gratings or, at least, we are working well inside the Talbot area, delimited by the blue triangle shown in Fig. 2(a). Other-

wise, this advantageous framework is no longer valid and the full system wave function has to be considered.

According to the previous statements, substituting Eq. (11) into (29) for the x coordinate yields

$$\dot{x} = \frac{1}{m} \frac{\sum_{i,j} p_i e^{-\sigma^2(p_i^2+p_j^2)/\hbar^2} \cos[(p_i - p_j)x/\hbar - (\omega_i - \omega_j)t]}{\sum_{i,j} e^{-\sigma^2(p_i^2+p_j^2)/\hbar^2} \cos[(p_i - p_j)x/\hbar - (\omega_i - \omega_j)t]}, \quad i, j = \pm 1, \pm 2, \dots \quad (30)$$

From this equation we can extract relevant information about the physical properties of the quantum trajectories (or, equivalently, their topology). Note that the velocity field (30) satisfies exactly the same symmetry conditions expressed by Eqs. (15) and (16). The particle motion is thus oscillatory, with the recurrences displayed by ρ_t occurring in those space regions where trajectories accumulate. However, unlike the disks depicted in Fig. 2(a), the trajectories associated with each single unit cell will remain inside it at any time and will never cross those coming from other unit cells: the particle motion is *bound*. This fact is a manifestation of the *noncrossing property* of Bohmian mechanics: trajectories can never pass through the same point on configuration space at the same time due to the single valuedness of the momentum field. This explains why the physics along each unit cell (or, by extension, the physics associated with infinite gratings) is so close to that observed in multimode cavities. The boundary periodic conditions give rise to the presence of nonphysical *impenetrable* walls at $x = \pm d/2$, where the velocity field (30) vanishes and therefore the corresponding quantum trajectories will be just straight lines. Due to the noncrossing property, these trajectories will act as (impenetrable) boundaries for particles coming from different neighboring slits. This is the Bohmian causal explanation for the Born-von Karman periodic boundary conditions. The same effect is also found for the trajectories starting at the center of the slits ($x = 0$), since the velocity field is also zero along this symmetry line. These trajectories evolve along two directions which are specular to one another (with respect to $x = 0$). Note that this goes beyond the classical-like picture provided by the disks associated with a multimode cavity in Fig. 2(b) in the sense that it adds a constraint of different nature to the types of motion that one can observe in quantum mechanics. Moreover, this behavior is regardless of the motion along the z direction (provided there is no coupling between both directions), where the corresponding equation of motion renders

$$z(t) = z_0 + v_z t. \quad (31)$$

That is, all particles display the same uniform rectilinear motion, as happens in classical mechanics, since the swarm of particles is basically guided by a plane wave.

If a size-limited grating is considered, after some time the trajectories will be out of the Talbot region, and therefore the description given above will no longer be applicable. Far beyond the grating, one can appeal to the Fraunhofer approximation in order to gain some insight on the topology of the trajectories. In such a case, introducing Eq. (19) into (29) leads to

$$\dot{x} \approx \frac{\hbar \kappa}{m} \frac{x}{z} = v_z \frac{x}{z}. \quad (32)$$

Assuming that the probability density is only significant along the quantized values of $x/z \approx \sin \theta$, where one observes the Fraunhofer principal maxima (we neglect the presence of secondary maxima), Eq. (32) becomes

$$\dot{x} \approx \ell v_z \frac{\lambda}{d}. \quad (33)$$

This assumption is equivalent to considering that the diffracted wave function consists of different independent plane waves, each one characterized by a quantized momentum $p_\ell = \ell(2\pi\hbar/d)$. This is a very important result that can be understood in terms of two different equilibrium regimes. The first equilibrium regime occurs in the Talbot/Fresnel region and is characterized by what we could call an *equilibrium of momenta*. That is, in this region the possible momenta satisfying a certain quantization condition are selected. This selection depends on the features defining the unit cell of the grating (or, in other words, the interaction potential between the grating and the diffracted particles). The second equilibrium regime, which we could call *equilibrium of configuration*, happens far beyond the grating, once the particle distribution remains with the same shape (regardless of spreading effects). The transition from the momentum to the configuration equilibrium is a direct consequence of the redistribution of momenta among the different particles contributing to ρ_t . These momenta make the swarm of particles to evolve in such a manner that, at a certain distance from the grating, it will separate in different beams, each moving with a different (average) momentum $p_\ell = \ell(2\pi\hbar/d)$. The equation of motion for the particles will then be

$$x(t) \approx x_0 + \frac{2\pi\hbar\ell}{md} t, \quad (34)$$

where $\ell = 0$ denotes the classical direction of motion. This contrasts with the remaining beams, which undergo a classical-like motion though they do not follow the real classical trajectory; the residual term involving \hbar is a clear indicator of the nonlocal behavior of quantum mechanics.²⁴ Nevertheless, as m increases, this deviation from the real classical motion gets smaller and smaller but never zero (as will be shown below).

The effects derived from the noncrossing property in periodic grating systems are equivalent to considering the presence of some effective impenetrable barriers. In the same way, the temporary accumulation of quantum trajectories in certain space regions could also be thought as the effect of an *effective quantum pressure*. For instance, the particles moving along an impenetrable (effective) barrier will keep their motion until those arriving from the central part of the initial wave packet will move towards $x = 0$, thus decreasing the “pressure” exerted on the former (the same effect has been discussed in multi-mode cavities¹⁹ or soft double slits¹³). The decrease of the quantum pressure is responsible for the appearance of Fraunhofer fringes; beyond the Talbot region, the particles feel a smaller pressure that allows them to get into different channels. After some time, particles reach the configuration equilibrium regime, where they move along well-defined channels, the well-known Bragg diffraction channels.

IV. SLIT ARRAYS

First we consider the dynamics due to slit arrays, where He atoms are the diffracted particles and the slits are described by Gaussian (transmission) functions.^{12,13} In Fig. 3(a) we can observe that, in accordance to the previous discussion in Sec. III, trajectories follow the flow characterizing ρ_t in Fig. 1(a). Note that here the *trajectory carpet* is not a one-piece structure, as happened with the Talbot carpet generated by ρ_t in Fig. 1(a), but it consists of many unit substructures (as many as slits have been considered). These structures are the causal effect of having indistinguishable unit cells. Moreover, trajectories exiting from one of the slits never cross those leaving the other slits, this being due to the noncrossing property described above. This can be better seen by looking at the enlargement presented in Fig. 3(b). In this plot we observe that initially the trajectories leave the slit in a diffusive manner towards each border of the slit. Since all the slits are identical (as well as their transmission function), these trajectories will feel in a short term the presence of bunches of trajectories coming from the neighboring slits. Then, the trajectories start bending until they move perpendicular to the slits for a while, pushed by the neighboring trajectories. This is a clear manifestation of the quantum pressure: the pressure exerted by bunches of trajectories moving in opposite directions gives rise to an effect similar to that of having an impenetrable (infinite) potential barrier. But the quantum pressure is also

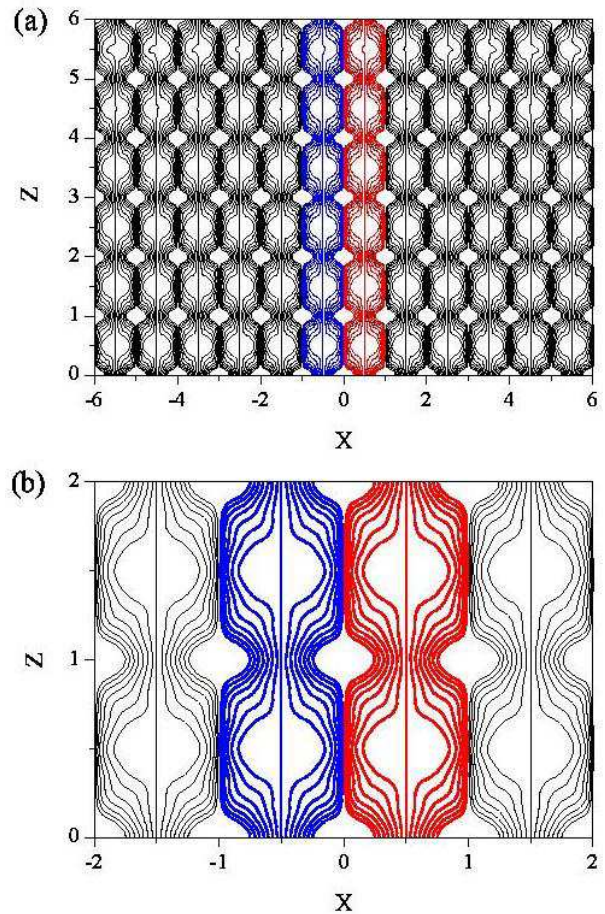


FIG. 3: (Color online) (a) Quantum trajectories associated with Fig. 1(a). Trajectories in different color indicate that though according to Fig. 1(a) the Talbot carpet seems to be a one-piece pattern, it is indeed constituted by many single bunches of trajectories arising from each slit and without crossing with those exiting from neighboring slits. (b) Enlargement of part (a) in the region close to the slits in order to show the correspondence with Fig. 1(b). In both panels, the x distance is scaled in units of the grating period d , and z in units of twice the Talbot distance ($2z_T$).

felt from the action of the trajectories coming from the same slit: those started with initial conditions closer to the center of the slit will push the other to move parallel; only when they start moving back again towards the central axis of the slit, the quantum pressure will decrease enough as to allow the outer trajectories to move again towards the original position of the slit. In this way, at $z = 2z_T$ we will recover again the initial pattern of a sum of Gaussians. It is interesting to stress that the maxima at $z = z_T$, shown in Fig. 1(b), have not the same structure as those at $z = 0$ or $z = 2z_T$; the trajectories contributing to the maxima at $z = z_T$ start from two different (neighboring) slits, while at $z = 2z_T$ only the trajectories started from the same slit will contribute to the corresponding maximum.

Provided the grating extends to infinity, the unit struc-

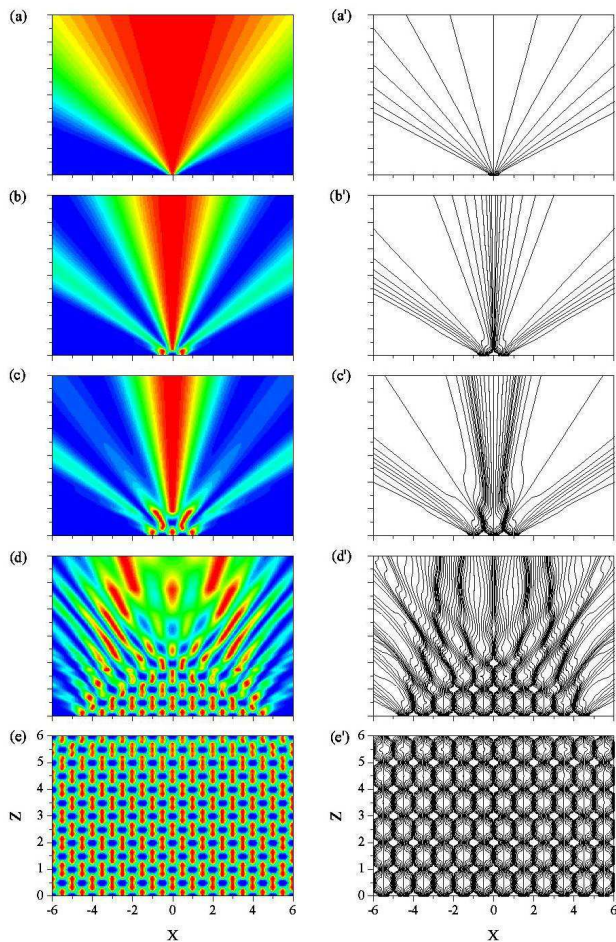


FIG. 4: (Color online) Left: Appearance of the Talbot carpet within a certain space region as the number of slits increases: (a) $N = 1$, (b) $N = 2$, (c) $N = 3$, (d) $N = 10$, and (e) $N = 50$. Right: Quantum trajectories corresponding to the cases shown in the left panels. In all panels, the x distance is scaled in units of the grating period d , and z in units of twice the Talbot distance ($2z_T$).

tures of the pattern seen in Fig. 3(a) repeat indefinitely. However, standard slit arrays have a limited size as well as the incident beam. Therefore, it is clear that the Talbot pattern will be observable only within certain boundaries; beyond these boundaries it will start to blur up, observing gradually the appearance of the Bragg diffraction channels.²⁷ Instead of going to this limit by propagating quantum trajectories further and further away, let us rather consider the case where we increase the number of slits progressively until reaching a number such that within a certain bound region we have the certainty of observing a Talbot pattern, but that further away we will only see Fraunhofer diffraction channels. This transition can be observed, from top to bottom, in Fig. 4 with both ρ_t (left) and the associated quantum trajectories (right).

As can be seen in Figs. 4(a) and 4(a'), the single slit case, the lack of neighboring trajectories allows the tra-

jectories to spread out in all directions with no bound and therefore no (Talbot) pattern can be observed. Free propagation of a Gaussian wave packet just means, according to this trajectory picture, that one can observe free motion (rectilinear and uniform) as in classical mechanics almost since the beginning of the propagation. In terms of the standard quantum mechanics, this means that ρ_t spreads linearly in time, but keeping its volume constant. This constant volume only means that the number of trajectories conserves although they are far apart from one another.

When two slits are considered, as in Figs. 4(b) and 4(b'), things change dramatically. From standard quantum-mechanical viewpoint we observe a channeling structure due to the interference of the two outgoing Gaussian wave packets. This is the Fraunhofer diffraction pattern. From the quantum trajectory viewpoint, though trajectories leave along those different channels (with a very low density of trajectories in between), the fact that the perpendicular semiplane behind the slits has been divided into two identical halves, where trajectories do not cross the half one dominated by the opposite slit is remarkable. There is a very strong quantum pressure exerted by the trajectories arising from each half along the symmetry axis of the system. Moreover, it is also worth commenting that very close to the slits a certain pattern, with two temporary maxima just behind the slits, is already present. In Figs. 4(c) and 4(c'), the three slit case, a similar pattern to that described when discussing Fig. 3(b) is observed. However, a Talbot pattern is still not formed because Fraunhofer diffraction channels emerge immediately.

From the previous comments we can then establish that the Talbot effect can be seen as a “partition” of the space as the number of slits increases because of the strong effect (acting as an infinite barrier) of the quantum pressure. This is confirmed when we go to $N = 10$ [see Figs. 4(d) and 4(d')] and $N = 50$ [see Figs. 4(e) and 4(e')]. Indeed, the existence of the quantum pressure leads to a sort of quantum equilibrium state in which the unit structures formed by the bunches of trajectories can coexist. Only when the quantum pressure starts decreasing, these units begin to blur up since the trajectories spread out the corresponding boundaries. Since this effect is similar to a dissipation, it could be called a *quantum trajectory dissipation* (though its nature is different to that of real dissipative phenomena). This “nonequilibrium” situation remains until a new equilibrium is established: the Fraunhofer regime. One must realize that the stationarity of the Talbot regime is only typical of this near field phenomenon. In general, near field or Fresnel phenomena are not stationary. Nonetheless, as we will see in the next section, one can still speak about a certain class of stationarity (in the momentum space) within the Fresnel diffraction regime different from that observed in a Talbot regime.

V. ATOM-SURFACE SCATTERING

Talbot patterns appear whenever one deals with any kind of infinitely periodic structure in which interference can be observed, and not only with gratings consisting of slit arrays. This is the case, for instance, of atom-surface scattering where the surface plays the role of the periodic grating.^{13,25} In Fig. 5 the formation of the Talbot pattern is plotted when we have a beam of He atoms illuminating ten unit cells of the Cu(110) surface at perpendicular incidence and energy $E_z = 21$ meV. This scattering system is described by a classical interaction potential $V(x, z) = V_M(z) + V_C(x, z)$, where

$$V_M(z) = D(1 - e^{-\alpha z})^2 - D \quad (35)$$

is a Morse potential, and

$$V_C(x, z) = De^{-2\alpha z} \left[0.03 \cos\left(\frac{2\pi x}{d}\right) + 0.0004 \cos\left(\frac{4\pi x}{d}\right) \right], \quad (36)$$

the coupling term between the two degrees of freedom. Here, $D = 6.35$ meV, $\alpha = 1.05 \text{ \AA}^{-1}$, and $d = 3.6 \text{ \AA}$ (as the aperture of the slits used before).^{26,27} The corrugation of the surface is very weak, as can be appreciated by the amplitudes of the cosine functions.

In order to make the plot clear, we have neglected the incident part of the trajectories and considered as before the evolution of those corresponding to the centroid line of the incoming wave parallel to the surface. As can be seen in Fig. 5(a), the pattern is very similar to that displayed by the ten-slit array plotted in Fig. 4(d'). This is because the corrugation of the surface is relatively weak. This can also be seen if we compare Figs. 5(b) and 3(b); though the latter has been obtained considering $N = 50$, the structure is similar in both cases (we are inside the Talbot area). Note, however, that the Talbot structure is slightly distorted and repeats a bit further away than twice the Talbot distance considered before ($2d^2/\lambda$). The reason for this shift and distortion is the attractive part of the interaction potential V , which causes a certain acceleration in the motion of the particles. This is the so-called *Beeby correction* in atom-surface scattering.¹⁰ In other words, only when the potential is flat, we can assume that $z_T = d^2/\lambda$. Otherwise, we should consider an effective Talbot distance,

$$\tilde{z}_T \equiv \frac{d^2}{\tilde{\lambda}(x, z)} = z_T \sqrt{1 - \frac{V(x, y)}{E_z}}, \quad (37)$$

where $\tilde{\lambda} = 2\pi\hbar/\sqrt{2m(E_z - V)}$. Taking into account that $V < 0$, it is clear that the square root factor in Eq. (37) will be greater than 1, and therefore $\tilde{z}_T > z_T$. The correction factor in Eq. (37) due to the presence of the well depth is $\sqrt{1 + D/E_z}$, and therefore we obtain $\tilde{z}_T/z_T = 1.14$, which is basically the discrepancy

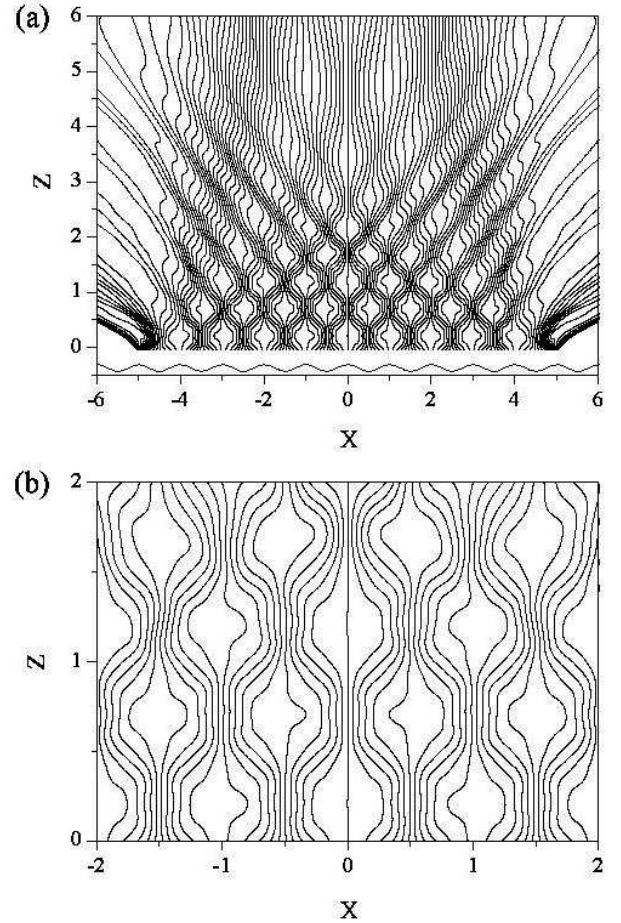


FIG. 5: (a) Quantum trajectories corresponding to the He-Cu(110) system at 21 meV and normal incidence. Only the emergent part has been plotted. (b) Enlargement of the trajectories shown in part (a). In both panels, the x distance is scaled in units of the Cu(110) unit cell d , and z in units of twice the Talbot distance for an N -slit grating ($2z_T = 2d^2/\lambda$).

observed in Fig. 5(b). Hence, within the context of atom-surface scattering, it would be appropriate to speak about the *Talbot-Beeby effect*, which gathers both the effects caused by the periodicity (depending on V_C) and those arising from the attractive part of the interaction (depending on V_M).

It is clear that since there is no infinite beam of He atoms illuminating the Cu surface, the quantum pressure will decrease as the atoms get further away from the surface, and the Talbot pattern will disappear. However, there is something very interesting in this kind of systems: one can extract already very important information about the diffraction peaks (experimentally detected at Fraunhofer distances) once the classical asymptotic region is reached ($V \simeq 0$). This is a nice manifestation of the effect mentioned above: the motion within the Fresnel region is governed by the momenta that will give rise later on to the different Fraunhofer diffraction channels. This has been easily proven by Sanz *et al.*²⁷ by computing

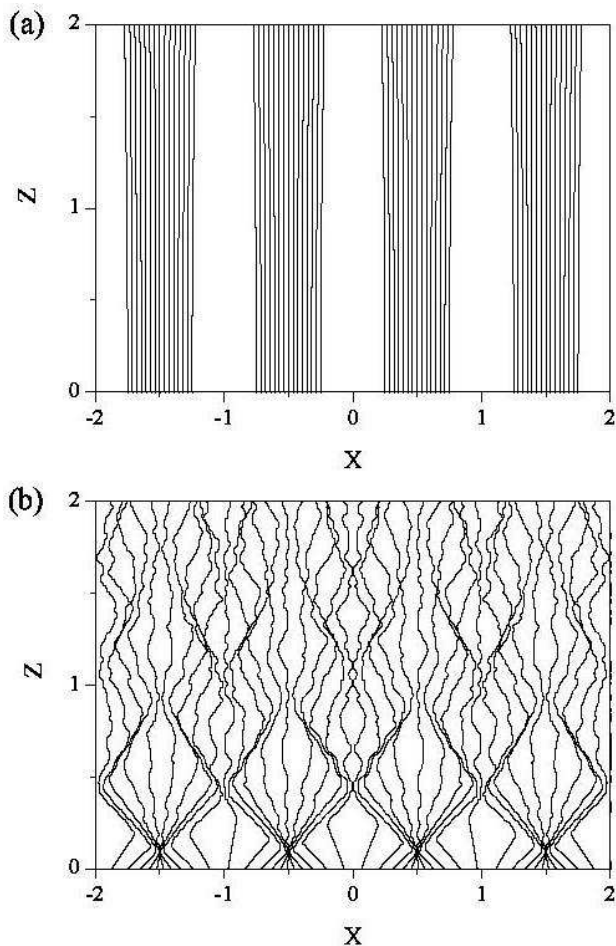


FIG. 6: Diffraction of a particle with a mass 500 times heavier than that of a He atom by (a) ten slits and (b) ten unit cells of the Cu(110) surface. In both panels, the x distance is scaled in units of the Cu(110) unit cell d , and z in units of twice the Talbot distance for an N -slit grating ($2z_T = 2d^2/\lambda$). Moreover, the perpendicular incidence energy is $E_z = 21$ meV in both cases.

the S -matrix elements in the classical asymptotic region and comparing them with the intensity calculated from quantum trajectories collected in the asymptotic region. A similar calculation for slit arrays by the same authors can be seen in Ref. 12. The Fraunhofer regime is reached very far from the region where the interaction potential V is negligible and increases its distance as the number of unit cells illuminated by the initial atomic beam is increased. Thus, for example, for ten unit cells the Fraunhofer regime is reached around 1000 Å.

VI. CORRESPONDENCE PRINCIPLE AND TALBOT EFFECT

As heavier impinging particles are considered, i.e., when we approach the classical limit, the behaviors observed in previous sections undergo dramatic changes,

approaching or resembling those expected classically. If instead of He atoms we consider a fictitious particle with a mass 500 times that of a He atom, it is clear that quantum effects should disappear or, at least, decrease. This is what one could think, mistakenly, when observing Fig. 6(a), where we have represented the diffraction of such particles by a grating consisting of ten slits. As can be seen, the trajectories are basically straight lines, what induces to think that no interference effects are present (neither Talbot nor Fraunhofer ones), but particles move tracing a simple rectilinear, uniform motion. Obviously, this is misleading; both the x and z directions are given in terms of the old d and z_T . However, if we replot this figure taking into account that now z_T has increased by a factor $\sqrt{m/m_{\text{He}}}$ (where m is the mass of the fictitious particle), we obtain again a Talbot pattern. And far away we would find the same Fraunhofer pattern as before. What has happened is that particles move now more slowly, and therefore the spreading of the corresponding bunches of trajectories will also be slower.

The previous result shows that quantum particles remain quantum even in the so-called classical limit;²⁸ one only needs to be patient and wait enough time in order to observe again the quantum phenomena (of course, unless the complexity of the system is so enormous that any quantum effect is imperceptible experimentally). However, what happens if instead of ten slits we illuminate ten cells of the Cu(110) surface with a beam of our fictitious particle? The answer appears in Fig. 6(b): now the topology displayed by the quantum trajectories tries to resemble that of the classical one, but the noncrossing principle holds. That is, since classical trajectories give rise to the appearance of two caustics (direction of maximum reflected intensity) at the so-called rainbow angles, the quantum trajectories will try to describe a similar structure, with the particularity that they cannot cross, and therefore, after tracing an almost straight line, they will be bounced backwards in relatively sharp angle, as seen in the lowest part of Fig. 6(b). Moreover, notice that, because of this motion, the laminarity of the flow described by the trajectories is lost; now the topology of the trajectories is more irregular, this leading to some crossings (though they occur at different times).

VII. CONCLUSIONS

To conclude, there are three important points in this work that are worth stressing. First, regardless of the gradual spreading of the partial wave function associated with each unit cell of a periodic grating, the corresponding initial swarms of quantum trajectories keep moving in a bound space region. To some extent, this is analogous to considering the trajectories moving inside a multimode cavity.^{13,19} Because of this effect, within the Talbot interferometry context, the superposition principle and the Born-von Karman boundary conditions in Bohmian mechanics have to be understood in a very different way as

they are in standard quantum mechanics. It is not simply the overlapping of a number of wave functions but allocation of identical copies of the same trajectory behavioral pattern. Second, this behavior is somehow similar to the classical behavior observed when studying periodic structures: all the information about the periodic structure can be obtained by simply studying the classical effects provoked by one of the periods although nonlocal effects are always present.¹² And third, the Talbot-Beeby effect is proposed to understand quantum trajectory carpets in

the presence of attractive interaction potentials.

Acknowledgements

This work has been supported by the Spanish Ministry of Education and Science under the project with reference No. FIS2004-02461 and for a “Juan de la Cierva” Contract awarded to one of the authors (A.S.S.)

-
- * Electronic address: asanz@imaff.cfnac.csic.es
† Electronic address: s.miret@imaff.cfnac.csic.es
- ¹ H.F. Talbot, *Philos. Mag.* **9**, 401 (1836).
 - ² L. Rayleigh, *Philos. Mag.* **11**, 196 (1881).
 - ³ M.S. Chapman, C.R. Ekstrom, T.D. Hammond, J. Schmiedmayer, B.E. Tannian, S. Wehinger, and D.E. Pritchard, *Phys. Rev. A* **51**, R14 (1995).
 - ⁴ L. Deng, E.W. Hagley, J. Denschlag, J.E. Simsarian, M. Edwards, C.W. Clark, K. Helmerson, S.L. Rolston, and W.D. Phillips, *Phys. Rev. Lett.* **83**, 5407 (1999).
 - ⁵ M. Berry, I. Marzoli, and W. Schleich, *Phys. World*, **14**, 7 (2001).
 - ⁶ D. Wójcik, I. Bialynicki-Birula, and K. Zyczkowski, *Phys. Rev. Lett.* **85**, 5022 (2000).
 - ⁷ M. Berry, *J. Phys. A* **29**, 6617 (1996).
 - ⁸ M.J.W. Hall, M.S. Reineker, and W.P. Schleich, *J. Phys. A* **32**, 8275 (1999).
 - ⁹ E.J. Amanatidis, D.E. Katsanos, and S.N. Evangelou, *Phys. Rev. B* **69**, 195107 (2004).
 - ¹⁰ J.L. Beeby, *J. Phys. C* **4**, L359 (1971).
 - ¹¹ J.T. Winthrop and C.R. Worthington, *J. Opt. Soc. Am.* **55**, 373 (1965).
 - ¹² A.S. Sanz, F. Borondo, and S. Miret-Artés, *J. Phys.: Condens. Matter* **14** 6109 (2002).
 - ¹³ R. Guantes, A.S. Sanz, J. Margalef-Roig, and S. Miret-Artés, *Surf. Sci. Rep.* **53**, 199 (2004).
 - ¹⁴ N.W. Ashcroft and N.D. Mermin, *Solid State Physics* (Saunders College, Philadelphia, 1976).
 - ¹⁵ M. Born and E. Wolf, *Principles of Optics* (Pergamon, New York, 1980).
 - ¹⁶ A.E. Kaplan, P. Stifter, K.A.H. van Leeuwen, W.E. Lamb, Jr., and W.P. Schleich, *Phys. Scrip.* **T76**, 93 (1998).
 - ¹⁷ A.E. Kaplan, I. Marzoli, W.E. Lamb, Jr., and W.P. Schleich, *Phys. Rev. A* **61**, 032101 (2000).
 - ¹⁸ M. Nest, *Phys. Rev. A* **73**, 023613 (2006).
 - ¹⁹ A.S. Sanz, *J. Phys. A* **38**, 6037 (2005); e-print arXiv:quant-ph/0412050.
 - ²⁰ D. Bohm, *Phys. Rev.* **85**, 166, 180 (1952).
 - ²¹ P.R. Holland, *The Quantum Theory of Motion* (Cambridge University Press, Cambridge, 1993).
 - ²² R.E. Wyatt, *Quantum Dynamics with Trajectories: Introduction to Quantum Hydrodynamics* (Springer, Berlin, 2005).
 - ²³ In Bohmian mechanics a wave function is uniquely associated with one single particle. However, in agreement to the statistical postulate of the standard quantum mechanics, this particle can have any initial position \mathbf{r}_0 with probability $\rho_0(\mathbf{r}_0)$. The results predicted by the standard quantum mechanics are reproduced by sampling all possible initial positions. This is equivalent to considering a system constituted by many *noninteracting* particles associated with the same wave function, and distributed according to $\rho_0(\mathbf{r})$.
 - ²⁴ A.S. Sanz and S. Miret-Artés, *J. Chem. Phys.* (submitted); *Chem. Phys. Lett.* (submitted); e-print arXiv:quant-ph/0703161.
 - ²⁵ A.S. Sanz and S. Miret-Artés, *Phys. Rep.* (accepted).
 - ²⁶ D. Gorse, B. Salanon, F. Fabre, A. Kara, J. Perreau, G. Armand, and J. Lapujoulade, *Surf. Sci.* **147**, 611 (1984); S. Miret-Artés, J. P. Toennies, and G. Witte, *Phys. Rev. B* **54**, 5881 (1996).
 - ²⁷ A.S. Sanz, F. Borondo, and S. Miret-Artés, *Phys. Rev. B* **61**, 7743 (2000).
 - ²⁸ A.S. Sanz, F. Borondo, and S. Miret-Artés, *Europhys. Lett.* **55** 303 (2001).